Joint Special Interest Group meeting between euspen and ASPE
Advancing Precision in Additive Manufacturing
Ecole Centrale de Nantes, France, September 2019
www.euspen.eu

Modelling of material deposition in big area additive manufacturing and 3D concrete printing

Raphaël Comminal [1], Marcin Piotr Serdeczny [1], Navid Ranjbar [1,2], Mehdi Mehrali [2], David Bue Pedersen [1], Henrik Stang [3], Jon Spangenberg [1]

[1]*Department of Mechanical Engineering, Technical University of Denmark, 2800 Kgs. Lyngby, Denmark*
[2]*Department of Health Technology, Technical University of Denmark, 2800 Kgs. Lyngby, Denmark*
[3]*Department of Civil Engineering, Technical University of Denmark, 2800 Kgs. Lyngby, Denmark*

rcom@mek.dtu.dk

Abstract
Big area additive manufacturing and 3D concrete printing are two technologies that upscale the material extrusion additive manufacturing concept to larger workpiece dimensions and higher build rates. This work presents a computation fluid dynamics model that simulates material extrusion and deposition using the software *FLOW-3D*. The numerical simulation is used to evaluate the cross-sectional shape of the printed beads. Several constitutive models have been considered to cover the wide range of material behaviours, including shear-thinning and visco-plasticity, that are expected in the flow of molten plastic and fresh concrete. The presence or absence of shear-thinning was found to have more influence on the cross-section of the bead than the actual values of the viscosity. The numerical results are also compared to the nominal bead's dimensions used in slicer softwares. The conclusion of this study is that the actual bead's dimensions can vary substantially from its nominal size, which is one of the phenomena that affects negatively the manufacturing precision.

Numerical simulation, material extrusion, big area additive manufacturing, 3D concrete printing, constitutive model

1. Introduction

Material extrusion additive manufacturing has promising innovative applications in the fields of Big Area Additive Manufacturing (BAAM) [1, 2] and 3D Concrete Printing (3DCP) [3, 4]. As examples, BAAM has been used to manufacture wind turbine blade moulds as well as prototype electric cars, while several demonstration buildings have been constructed across the World using 3DCP. Both technologies are based on the same concept of layered material extrusion as desktop 3D printers, except that their workpiece dimensions and their build rates are upscaled by factors of 10x to 100x. To achieve the latter, BAAM machines typically use a screw extruder to melt and extrude thermoplastic pellets, whereas 3DCP machines operate on fresh concrete that is pumped into a pipe connected to the extrusion nozzle. In both cases, the extrusion nozzle is generally mounted on a gantry or an industrial robot arm, in order to control precisely the deposition path.

Nevertheless, upscaling the nozzle diameter and the layer height is detrimental to the printing resolution and the surface finish of the manufactured components. For both processes, deviations in the dimensions of the deposited bead from its nominal size have detrimental consequences on the dimensional accuracy and the structural integrity of the parts. In the case of BAAM, the ability of printing complex shapes with cavities, overhangs, and bridging layers highly depends on the thermal and rheological properties of the rubbery state of the plastic [5]. In the case of 3DCP, the buildability of large-scale concrete structures (i.e. the ability to print fresh concrete on top of existing layers without deforming them) is influenced by the early age mechanical properties of the materials [6]. Thus, the development of concrete formulations with suitable rheological properties is one of the key aspect to the success of 3DCP [7].

The current work focuses on simulating the flow of the printed material exiting the extrusion nozzle and being deposited onto the build surface. The numerical simulations are used to predict the height and width of the printed bead. The simulations presented here differ from previous works [8-11] by the dimensions of the nozzle, the layer height, and the magnitude of the build rate, which are upscaled in order to represent BAAM and 3DCP. Moreover, different constitutive models are used to take into account the shear-thinning and visco-plastic phenomena of the extruded material.

2. Numerical model

2.1. Governing equations

The dynamics of the extrusion-deposition flow is governed by the conservation of mass and momentum. The material is assumed to be incompressible, thus the flow follows the continuity equation:

$$\frac{\partial \boldsymbol{u}_j}{\partial \boldsymbol{x}_j} = 0, \tag{1}$$

where $\boldsymbol{u}$ is the local velocity vector and $\boldsymbol{x}$ is a position vector within the flow. The Cauchy momentum equation reads:

$$\rho\left(\frac{\partial \boldsymbol{u}_i}{\partial t} + \boldsymbol{u}_j\frac{\partial \boldsymbol{u}_i}{\partial \boldsymbol{x}_j}\right) = -\frac{\partial p}{\partial \boldsymbol{x}_i} + \frac{\partial \boldsymbol{\sigma}_{ij}}{\partial \boldsymbol{x}_j} + \rho \boldsymbol{g}_i, \tag{2}$$

where ρ is the density of the material, p is the pressure, $\boldsymbol{\sigma}$ is the constitutive stress tensor and $\boldsymbol{g}$ is the gravitational acceleration vector. The left-hand side of eq. (2) corresponds to the rate of change in momentum, while the right-hand side contains the sum of all the internal and external forces applied to the material. The index i in eq. (2) refers to each of the three

components of the momentum equation, whereas the index j in both eq. (1) and eq. (2) is a summation index.

The constitutive stress of the extruded material is modelled with a generalized Newtonian fluid model:

$$\boldsymbol{\sigma}_{ij} = 2\eta_{\mathrm{app}}(\dot{\gamma})\boldsymbol{D}_{ij}, \tag{3}$$

where

$$\boldsymbol{D}_{ij} = \frac{1}{2}\left(\frac{\partial \boldsymbol{u}_i}{\partial \boldsymbol{x}_j} + \frac{\partial \boldsymbol{u}_j}{\partial \boldsymbol{x}_i}\right) \tag{4}$$

is the rate of deformation tensor, and η_{app} is the apparent viscosity of the material that depends on the magnitude of the shear rate $\dot{\gamma}$, defined as:

$$\dot{\gamma} = \left(2\sum_{i,j}\boldsymbol{D}_{ij}\boldsymbol{D}_{ij}\right)^{1/2}. \tag{5}$$

A regularized Herschel-Bulkley fluid model was chosen to describe the apparent viscosity, as it can fit the rheological data of both molten thermoplastic [12] and fresh concrete [13]:

$$\eta_{\mathrm{app}}(\dot{\gamma}) = \begin{cases} \eta_0, & \dot{\gamma} \le \dot{\gamma}_0 \\ \dfrac{\tau_0}{\dot{\gamma}} + K\dot{\gamma}^{n-1}, & \dot{\gamma} > \dot{\gamma}_0 \end{cases}, \tag{6}$$

where τ_0 is a yield stress, n is a power-law index and K is the consistency index. The critical shear rate $\dot{\gamma}_0$ is a regularization parameter introduced to avoid having an infinite zero-shear viscosity, as $\lim_{\dot{\gamma}\to 0}(\tau_0/\dot{\gamma} + K\dot{\gamma}^{n-1}) = +\infty$. Moreover, the maximum cut-off value of the viscosity is $\eta_0 = \tau_0/\dot{\gamma}_0 + K\dot{\gamma}_0{}^{n-1}$. The Herschel-Bulkley fluid model yields a Bingham plastic fluid when $n = 0$, and a power-law fluid when $\tau_0 = 0$. If both $n = 0$ and $\tau_0 = 0$, the model reduces to a Newtonian fluid (with the constant viscosity $\eta_{\mathrm{app}} = K$).

2.2. Numerical simulations

The geometry of the numerical simulation includes a cylindrical extrusion nozzle, with an inner diameter D = 25 mm and an outer diameter of 40 mm, which corresponds to a nozzle dimension used in 3DCP (for BAAM, the largest nozzle diameters are about 10 mm). The extrusion nozzle was positioned at a height L = 12.5 mm above the build surface. The material was extruded from the nozzle with a build rate of 4.91 cm^3/s, which corresponds to an average velocity (i.e. a volumetric flux) U = 10 mm/s within the cross-section of the nozzle. Moreover, the extrusion nozzle was modelled as a moving object with a linear toolpath of 200 mm, as represented in figure 1. The velocity of the nozzle was prescribed to V = 10 mm/s.

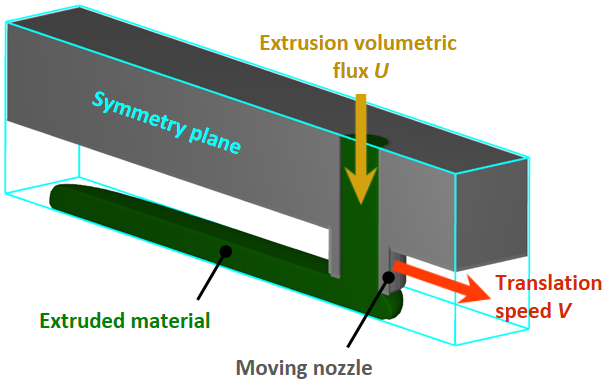

Figure 1. Geometry and boundary conditions of the computational domain. The extruded material is represented after the nozzle has already travelled 180 mm.

The three-dimensional flow domain was discretized with a uniform Cartesian mesh with a resolution of 1 mm. The solid objects within the flow domain are represented by the immersed boundary method. By virtue of symmetry, only half of the domain is simulated.

The governing equations of the flow are solved with the finite volume method, using the computational fluid dynamics software *FLOW-3D* that has previously been used with success to simulate other applications with both cementitious and polymer materials [14, 15]. The extruded material is modelled as a single fluid phase with a sharp free surface whose position is tracked by the volume-of-fluid method.

The numerical simulation was executed for different constitutive models whose material parameters are provided in table 1. The apparent viscosity for each of these constitutive models is also represented in figure 2 as a function of the shear-rate. The material had a density of 2.11 kg/dm^3.

Table 1. Numerical values of the constitutive parameters.

Constitutive model	n	K/Pa · s^n	τ_0/Pa	$\dot{\gamma}_0/s^{-1}$
Newtonian	1	10000	0	0
Power-law	0.5	10000	0	0.001
Herschel-Bulkley	0.5	1000	1480	0.1
Bingham	1	21.1	1480	0.1

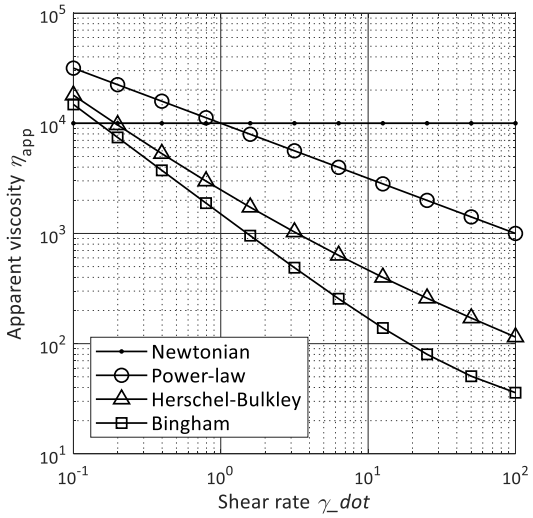

Figure 2. Viscosity function of the different constitutive models with the material parameters provided in table 1.

3. Results and discussions

At the end of the numerical simulations, the free-surface of the extruded material is monitored to determine the cross-section of the printed bead. Figure 3 represents the different cross-sections obtained with all four constitutive models as well as the theoretical oblong shape assumed by the slicing softwares. The theoretical bead's width W_{th} and bead's height H_{th} are obtained from the volume conservation and by assuming that the bead's height equals the layer height [8]:

$$W_{\mathrm{th}} = \frac{\pi}{4}\frac{U}{V}\frac{D^2}{L} + L\left(1 - \frac{\pi}{4}\right), \tag{7}$$

$$H_{\mathrm{th}} = L. \tag{8}$$

The cross-section obtained with the Newtonian fluid model differs the most from the other constitutive models. The cross-section of the shear-thinning materials (i.e. the power-law, Herschel-Bulkley and Bingham fluids) appears higher and less wide than for the Newtonian fluid that has a constant viscosity. This could be explained by the fact that the laminar flow of the

Newtonian fluid, which has a parabolic velocity profile inside the extrusion nozzle, requires more rearrangements at the nozzle's exit, enhancing the side deposition flows. In contrast, the shear-thinning fluids have fully developed flow profiles closer to plug flows [16]. The results suggest that the extrusion-deposition flow is more affected by the presence or absence of shear-thinning than the magnitude of the apparent viscosity (the flow is in a creeping flow regime [8] where the inertial effects are small compared to the viscous forces).

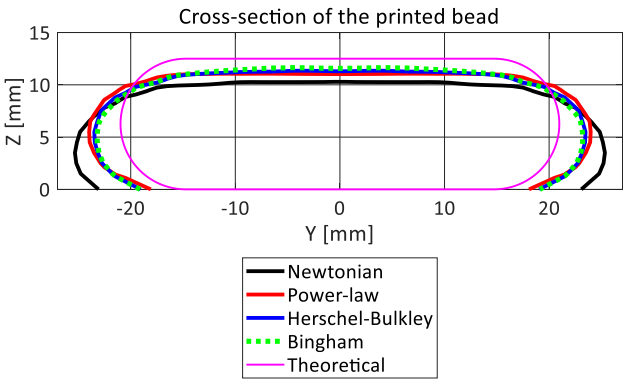

Figure 3. Cross-section of the printed bead for the different constitutive models.

The relative deviations of the bead's dimensions from those of the theoretical oblong shape are reported in figure 4. The data in figure 4 also include the numerical results published in [8], for the 3D printing of polymers with a desktop 3D printers, where the extrusion-deposition flow was modelled with the Newtonian fluid model. In the numerical simulations, the beads are lower than the layer height, and their deviations from the theoretical oblong shape are between 10 % to 20 % for the bead's width and -7 % to -18 % for the bead height, depending on the constitutive model. Such differences between the actual bead's dimensions and the approximate theoretical values have also been observed experimentally for the 3D-printing of thermoplastic strands with a desktop 3D printer [9].

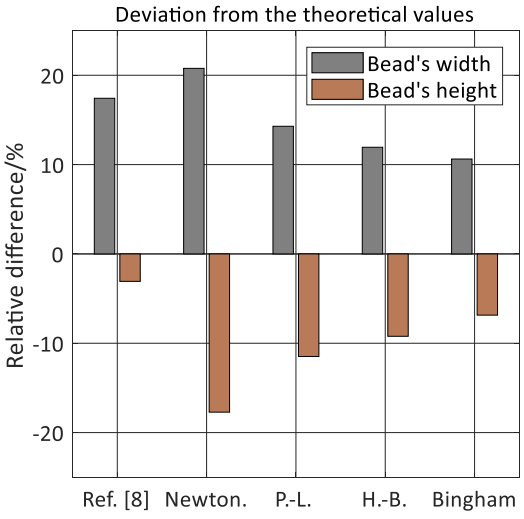

Figure 4. Deviation of the bead's width and height from the approximate theoretical values, for the different constitutive model.

5. Conclusions

Computational fluid dynamic models have been used to simulate the material extrusion in BAAM and 3DCP, whose dimensions and build rates are upscaled as compared to desktop 3D printers. The simulations include a moving nozzle that prints material along a straight line. Several constitutive models formulated as generalized Newtonian fluids have been tested to represent the shear-thinning and visco-plastic behaviour of molten plastic and fresh concrete.

The numerical simulations give predictions of the shape of the printed beads. For the constitutive models considered in this study, the presence or absence of shear-thinning effect has a more important influence on the cross-section of the beads than the magnitude of the apparent viscosity. The results for the different shear-thinning fluids yielded similar bead's cross-sections, despite the differences their constitutive parameters. Moreover, the simulations show that the bead's dimensions substantially differ from the theoretical values used by the slicer software to calculate the tool path of the printing nozzle.

Differences between the actual and nominal size of the printed beads is one of the effects that deteriorate precision in BAAM and 3DCP. Numerical simulations can be a complementary tool to experimental observations, to investigate different phenomena influencing the precision of material extrusion additive manufacturing. Future work will extend the simulations to additional constitutive models such as the elasto-visco-plastic fluid models that include elastic deformations. Numerical simulations could also be used to model the deformations of the printed part due to gravity, thermal shrinkage of plastics, and setting of concrete materials.

Acknowledgements

The authors would like to acknowledge the support of the Innovation Fund Denmark (Grant no. 8055-00030B: Next Generation of 3D-printed Concrete Structures) and the Danish Council for Independent Research (DFF) | Technology and Production Sciences (FTP) (Contract no. 7017-00128). The work of N. Ranjbar received funding from the European Union's Horizon 2020 research and innovation program under the Marie Sklodowska-Curie grant agreement no. 713683 (COFUNDfellowsDTU).

References

[1] Holshouser C et al. 2013 Out of bounds additive manufacturing *Adv. Mater. Processes* **171** 15-7.

[2] Love L J, Duty C E, Post B K, Lind R F, Lloyd P D, Kunc V, Peter W H and Blue C A 2015 Breaking barriers in polymer additive manufacturing *SAMPLE Conference (Baltimore, MD, 19–20 May 2015)*.

[3] Bos F, Wolfs R, Ahmed Z and Salet T 2016 Additive manufacturing of concrete in construction: potentials and challenges of 3D concrete printing *Virtual Phys. Prototyp.* **11** 209-25.

[4] Wangler T, Roussel N, Bos F P, Salet T A M and Flatt R J 2019 Digital concrete: a review *Cem. Concr. Res.* **123** 105780.

[5] Roschli A, Gaul K T, Boulger A M, Post B K, Chesser P C, Love L J, Blue F and Borish M 2019 Designing for big area additive manufacturing *Addit. Manuf.* **25** 275-85.

[6] Panda B, Lim J H and Tan M J 2019 Mechanical properties and deformation behaviour of early age concrete in the context of digital construction *Composites Part B* **165** 563-71.

[7] Roussel N 2018 Rheological requirements for printable concretes *Cem. Concr. Res.* **112** 76-85.

[8] Comminal R, Serdeczny M P, Pedersen D B and Spangenberg J 2018 Numerical modeling of the strand deposition flow in extrusion-based additive manufacturing *Addit. Manuf.* **20** 68-76.

[9] Serdeczny M P, Comminal R, Pedersen D B and Spangenberg J 2018 Experimental validation of a numerical model for the strand shape in material extrusion additive manufacturing *Addit. Manuf.* **24** 145-53.

[10] Serdeczny M P, Comminal R, Pedersen D B and Spangenberg J 2019 Numerical simulations of the mesostructure formation in material extrusion additive manufacturing *Addit. Manuf.* **28** 419-29.
[11] Comminal R, Serdeczny M P, Pedersen D B and Spangenberg J 2019 Motion planning and numerical simulation of material deposition at corners in extrusion additive manufacturing *Addit. Manuf.* (in press).
[12] Mackay M E, Swain Z R, Banbury C R, Phan D D and Edwards D A 2017 The performance of the hot end in a plasticating 3D printer *J. Rheol.* **61** 229-36.
[13] De Larrard F, Ferraris C F and Sedran T 1998 Fresh concrete: a Herschel-Bulkley material *Mater. Struct.* **31** 494-8.
[14] Jacobsen S, Cepuritis R, Peng Y, Geiker M R and Spangenberg J 2013 Visualizing and simulating flow conditions in concrete form filling using pigments *Constr. Build. Mater.* **49** 328-42.
[15] Spangenberg J, Uzal A, Nielsen M W and Hattel J H 2018 A robustness analysis of the bonding process of joints in wind turbine blades *Int. J. Adhes. Adhes.* **85** 281-5.
[16] Comminal R, Pimenta F, Hattel J H, Alves M A and Spangenberg J 2018 Numerical simulation of the planar extrudate swell of pseudoplastic and viscoelastic fluids with the streamfunction and the VOF methods *J. non-Newton. Fluid Mech.* **252** 1-18.